Analyst

ROYAL SOCIETY OF CHEMISTRY

PAPER

View Article Online
View Journal | View Issue

Cite this: *Analyst*, 2021, **146**, 5255

Three dimensionally printed nitrocellulose-based microfluidic platform for investigating the effect of oxygen gradient on cells†

Ping Liu,[a,b] Longwen Fu,[b,c] Zhihua Song,[d] Mingsan Man,[b] Huamao Yuan,[e,c] Xiaoli Zheng,[a] Qi Kang,[a] Dazhong Shen, *[a] Jinming Song,[e,c] Bowei Li *[b,c] and Lingxin Chen *[b,c]

In this article, we present a novel nitrocellulose-based microfluidic chip with 3-dimensional (3D) printing technology to study the effect of oxygen gradient on cells. Compared with conventional polydimethylsiloxane (PDMS) chips of oxygen gradient for cell cultures that can only rely on fluorescence microscope analysis, this hybrid nitrocellulose-based microfluidic platform can provide a variety of analysis methods for cells, including flow cytometry, western blot and RT-PCR, because the nitrocellulose-based chips with cells can be taken out from the growth chambers of 3D printed microfluidic chip and then used for cell collection or lysis. These advantages allow researchers to acquire more information and data on the basic biochemical and physiological processes of cell life. The effect of oxygen gradient on the zebrafish cells (ZF4) was used as a model to show the performance and application of our platform. Hypoxia caused the increase of intercellular reactive oxygen species (ROS) and accumulation of hypoxia-inducible factor 1α (HIF-1α). Hypoxia stimulated the transcription of hypoxia-responsive genes vascular endothelial growth factor (VEGF) and induced cell cycle arrest of ZF4 cells. The established platform is able to obtain more information from cells in response to different oxygen concentration, which has potential for analyzing the cells under a variety of pathological conditions.

Received 25th May 2021,
Accepted 24th July 2021

DOI: 10.1039/d1an00927c

rsc.li/analyst

1. Introduction

Oxygen is fundamental to biological processes, when the supply of oxygen is low, it can lead to a condition known as hypoxia.[1] Hypoxia can alter immune responses, increase disease and reduce growth of individual organisms,[2,3] in brief, hypoxia influences life from genes to ecosystem responses.[4]

In order to study the behaviour of cells under low oxygen concentration, hypoxic workstations perfusion chambers and hypoxic culture chambers have been used to create hypoxic environments for cells.[5] However, these devices are expensive, and they do not provide physiological hypoxic gradients. To overcome these shortcomings, the hypoxic platforms of microfluidic chip have been developed. Microfluidic chips have the advantages of miniaturization, reduced reagent, and low energy consumption. Due to the advancement of microfluidic techniques, a number of microfluidic devices capable of controlling oxygen content have been developed, including devices relying on oxygen scavenging chemicals,[6–9] multi-gas incubator[10] and gaseous perfusion.[11–13] Among these devices, gas perfusion is the most direct and popular way for oxygen control, because the viscosity of gas is low, it can be mixed quickly. Moreover, the gas flow can be driven by pressure tanks, which eliminates the use of injection pump.[5] The advantages of simplicity and convenience make gas perfusion a good choice for oxygen control.

Polinkovsky *et al.* presented a multilayer microfluidic device of oxygen gradient based on gas perfusion. Two gases (N_2 and O_2) flow through a three-step on-chip mixing channel network, which culminates in nine discrete O_2 concentration varying linearly between 0 and 100%. The gas layer flow over the

[a]*College of Chemistry, Chemical Engineering and Materials Science, Key Laboratory of Molecular and Nano Probes, Ministry of Education, Shandong Normal University, Jinan 250014, China. E-mail: dzshen@sdnu.edu.cn*
[b]*CAS Key Laboratory of Coastal Environment Processes and Ecological Remediation, The Research Center for Coastal Environment Engineering and Technology, Yantai Institute of Coastal Zone Research, Chinese Academy of Sciences, Yantai 264003, China. E-mail: bwli@yic.ac.cn, lxchen@yic.ac.cn*
[c]*Center for Ocean Mega-Science, Chinese Academy of Sciences, Qingdao 266071, China*
[d]*School of Pharmacy, Key Laboratory of Molecular Pharmacology and Drug Evaluation (Yantai University), Ministry of Education, Yantai University, Yantai, 264005, China*
[e]*Key Laboratory of Marine Ecology and Environmental Sciences, Institute of Oceanology, Chinese Academy of Sciences, Qingdao, China*
†Electronic supplementary information (ESI) available. See DOI: 10.1039/d1an00927c

growth chambers, making the medium in the growth chambers contain different concentrations of oxygen.[14] This device presents a way to produce different oxygen concentrations using one platform. But this multilayer microfluidic device is made of highly gas-permeable polydimethylsiloxane (PDMS) by photolithography, which needs multiple production steps, substantial human labor and high cost of equipment. Moreover, the analysis of cells in the growth chamber mainly depends on the fluorescence microscope, which makes some physiological changes impossible to detect.

3D printing technology has recently attracted attention as a method to manufacture microfluidic systems.[15–17] Compared to traditional fabrication techniques of microfluidic chip such as the soft lithography, 3D printing has the advantages of one-step production, low costs and high throughput.[17] So recent years 3D printing has been widely used in manufacture of the gradient generator, micromixer, droplet extractor, and devices of isotachophoresis.[18,19]

Paper is a cellulosic and porous material, it has many unique features, such as high biocompatibility, low cost, ease of handling, and facilely integrated with other devices.[20–27] Over the past few years, paper has been used in various fields for cell research, including invasion assays of cancer cells,[28] stem cell differentiation,[29] three dimensional cell culture,[30] cardiac ischemia construction and single cell analysis.[31,32] These reported paper microfluidic devices were generally manufactured with filter paper whose pore size was larger than 2 μm, however, large pore size made the cells leaking out of the filter paper easily. Nitrocellulose membrane (NC membrane) is a kind of paper substrate made from pure cellulose nitrate, and has quite small (<0.45 μm) and uniform pore size. The surface of the NC membrane is much smoother than filter paper, and the hydrophilicity of NC membrane is strong.[33,34] The above characters highlight the flexibility of NC membrane as a substrate for cell culture.

Herein, we used nitrocellulose membrane (NC membrane) to make paper-based chip and combined with 3D printing technology to construct stable oxygen gradient platform for cell culture. The cells of fish who suffers from environmental hypoxia in water was used as a model to show the performance and application of our platform. The effects of hypoxic on the cell cycle, signal molecule and gene expression of fish cells were investigated. This hybrid platform of cell culture provides an excellent way to research the effect of hypoxia on cells with minimal equipment. Moreover, the established platform offers a variety of analytical methods for cells on it, which will greatly expands the application field of microfluidic chips and has the potential to be a versatile platform for studying cellular responses under various oxygen gradients.

2. Experimental

2.1 The design and manufacture of 3D printed device

The 3D printed device was designed in Auto CAD. It contained two layers including a bottom plate and a top cover (Fig. S1†). A gas-mixing microchannel network embedded in the bottom plate. The microchannel network consisted of two kinds of pipes, serpentine pipes were used to mix the gas by diffusion, and horizontal pipes were used to redistribute gas.[14,35] The diameter of serpentine channels was 2.0 mm, and horizontal channels had diameter of 4 mm. There were two gas inlets with the diameter of 1.8 mm at the top of the networks,[36,37] and five growth chambers were connected to the gas channel network, whose dimension were 12 mm wide, 12 mm long and 9 mm deep, respectively. A cover plate with dimension of 90 mm length, 26 mm width and 2 mm thickness was put above the growth chambers. Twelve threaded holes were penetrated the bottom plate and top cover to install screws, which make sure two pieces were in closed contact. The channel with 2.0 mm in diameter was connected to each growth chamber as the outlet of gas. Then the microfluidic chip was printed on a 3D printer with transparent resin according to the design drawing (Future Factory Company, Shenzhen, China).

2.2 Verify the efficiency of 3D printing chip to generate oxygen gradients

To calculate the profile of oxygen gradient in the cell culture chambers of 3D printed microfluidic chip, an oxygen fluorescence probe named ruthenium tris (2,2′-bipyridyl) dichloride hexahydrate (RTDP) (5 mg mL^{-1}) was exploited in the experiments.[38] Added 300 μL solution of RTDP into the cell growth chambers, then assembled the chip with screws. One of the gas inlets connected to a N_2 tank through a gas buffer bottle, the other connected to a compressed air tank also through a gas buffer bottle. The pressure was set at 80 psi for both gases. The growth chambers were numbered 1–5 from N_2 to air (Fig. 1). As shown in Fig. S4,† the gas in the cell culture chamber equilibrated to a steady state in about 23 min. So, let the system equilibrate for 30 min, then detected oxygen concentration in the cell culture chambers. The solution in each cell culture chamber was imaged by laser scanning confocal microscope (Olympus FV1000, Japan) with excitation wavelength 488 nm and collection wavelength 500–600 nm. The fluorescence intensity of the images was quantified using image processing software of laser scanning confocal microscope. The oxygen tension in each culture chamber was calculated using the respective fluorescence intensity according to Stern–Volmer equation:[39]

$$\frac{I_0}{I} = 1 - K_q[O_2] \quad (1)$$

I_0 represents the value of fluorescence intensity without oxygen, I indicates the fluorescence intensity in the presence of different oxygen concentration, and K_q represents quenching constant.[40] In order to calibrate $[O_2]$, I_0 and I_{air} (the value of fluorescence intensity in 0% and 21% oxygen content) were used. In this way, quenching constant K_q can be obtained by changing eqn (1):

$$K_q = \frac{I_0 - I_{21} + I_{21}[O_2]_{air}}{I_{21}[O_2]_{air}} - 1 \quad (2)$$

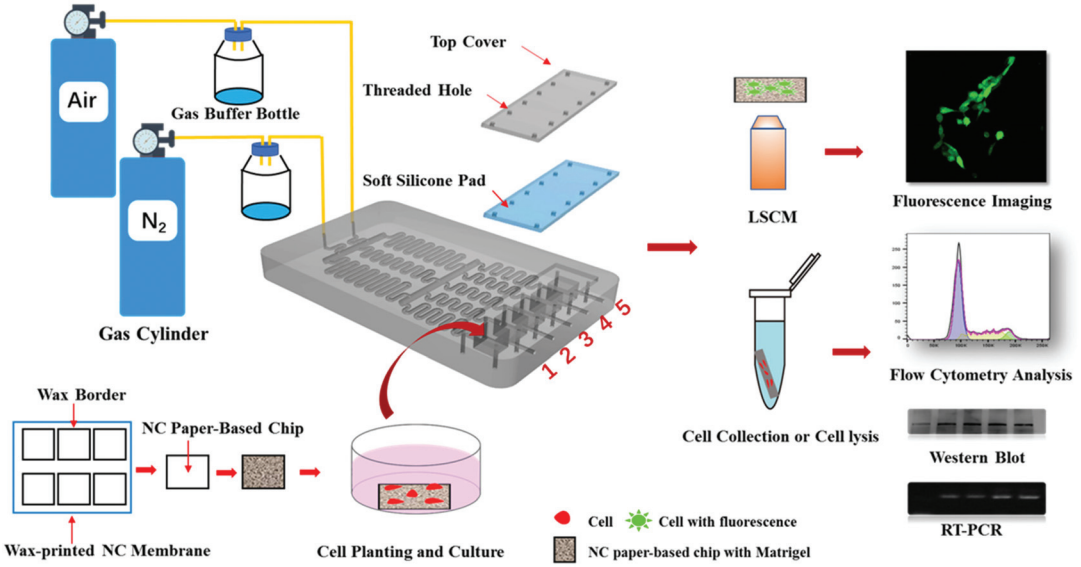

Fig. 1 Working schematic of microfluidic chip oxygen gradient cell culture platform. Zebrafish ZF4 cells were seeded onto the NC paper-based chips pre-coated with Matrigel and cultured in the cell culture plate. The NC paper-based chips with fish cells were put into the medium of culture chambers. The two pieces of the chip and soft silicone pad were assembled with screws. Compressed air and N_2 were injected into the microfluidic chip through the gas buffer bottles. The cells were cultured in the oxygen gradient microfluidic chip for a period of time according to the experimental requirements, then disassembled the 3D-printed chip and took out the NC paper-based chips for processing and analysis of cells.

where $[O_2]_{air}$ is 21%. Consequently, the $[O_2]$ in every cell culture chamber could be calculated on the base of the measured fluorescence intensity value I and obtained values of K_q using eqn (1).[13]

2.3 Manufacture of the paper-based chip in NC membrane

Freehand software was used to design the square array of chip. The side length of the square hydrophilic area was 10 mm. The wax microstructures was printed onto the surface of the nitrocellulose (NC) membrane (0.45 μm, Beyotime) with a wax printer (Xerox Company, Japan) as previous reports.[41,42] The wax-printed NC membrane were then roasted at 125 °C for 5 min, which made the wax to penetrate to the other side of the of NC membrane.[33] We cut out the square chips from the NC membrane layer with scissors (Fig. S5†), then sterilized the NC paper-based chips under ultraviolet lamp for 4 h, and sterilized the other side for 4 h.

2.4 Fish cells culture and identification in the 3D printed chip

To check the growth state of cells in the 3D printed chip, zebrafish embryonic cell line ZF4 was used. The culture methods for ZF4 cells were described in the support information. The NC paper-based chips were pre-coated with Matrigel (diluted 1 : 40) at 4 °C for 12 h, then incubated at 37 °C for 1 h to solidify the Matrigel.[34] Put the NC paper-based chips into a cell culture plate of 24 wells, then ZF4 cells were seeded onto the NC paper-based chips at 1×10^4 cells per cm^2, and the cells were incubated in a culture incubator (28 °C, 5% CO_2) overnight for ZF4 cells attaching to the NC paper-based chips. The 3D-printed chip was soaked in 75% alcohol for 30 minutes to sterilize, and washed three times in deionized water. It was then air-dried in a super clean bench. 300 μL culture medium was added to each culture chamber of the 3D-printed chip, then the NC paper-based chips with cells were put into the growth chambers, or they were transferred to other wells of 24-well plate as controls. After the cells in the 3D-printed chip and 24-well plate were cultured for 12 and 24 hours, the cell viability was performed using live cell imaging and cell proliferation assays. For live cell imaging assay, the cells were stained with NucBlue Live Cell Stain Ready Probes reagent (Invitrogen, USA) and imaged on laser scanning confocal microscope. Cell proliferation assay was based Cell Counting kit-8 (CCK-8, Beyotime, China), when the reaction was completed, 100 μL liquid from each group was removed to a 96-well plate, the absorbance at 450 nm was detected by a microplate reader (Tecan, Austria).

2.5 Fish cells cultured on the platform with oxygen gradient

ZF4 cells were seeded on the NC paper-based chips as described above, then the NC paper-based chips with fish cells were put into growth chambers of 3D printed chip, then the two pieces of the chip and soft silicone pad were assembled with screws. Compressed N_2 and air were injected into the microfluidic chip through the gas inlets at the pressure of 80.0 psi. The whole platform was transferred to a cell culture incubator (28 °C and 5% CO_2) and then cultured for a period of time according to the experimental requirements. When the time was up, disassembled the 3D-printed chip and took out the NC paper-based chips for processing and analysis of cells.

2.6 Evaluation of cellular oxygen levels

Cellular oxygen levels was evaluated with Image-iT ™ Green Hypoxia Reagent.[43] The NC paper-based chips were put into the growth chambers of the 3D printed chip. Each chamber had fresh medium with the Image-iT ™ Green Hypoxia Reagent of 5 μM. ZF4 cells were exposed to different oxygen tensions for 4 h in the hypoxic platform.[44] The fluorescence images of cells on the NC paper-based chips were detected on the LSCM (laser scanning confocal microscope), or the cells were digested and harvested for Flow Cytometry analysis after the cells were washed three time with phosphate buffered saline.

2.7 Detection of cellular reactive oxygen species (ROS)

ZF4 cells (about 1.0×10^5) on the NC paper-based chips were cultured for 4 h on the platform of oxygen gradient. The NC paper-based chips were put into EP (Eppendorf) tubes, and were washed in phosphate buffered saline for three times, then digested and collected the cells. The cells were stained with ROS probe DCFH-DA (Beyotime, China) at a final concentration of 10 μM in 28 °C for 30 minutes. Cellular fluorescence was analyzed by flow cytometry (BD Aria I) after washing by phosphate buffered saline for three times. The data were analyzed by Diva software (BD, USA).

2.8 Protein extraction and western blotting

ZF4 cells on the NC paper-based chips were cultured for 4 h in the platform of oxygen gradient. We took the NC paper-based chips out from the growth chambers of 3D printed chip with tweezers and put them into EP tubes. After the cells were washed with phosphate buffered saline, they were lysed for 30 minutes on the ice with cell lysis buffer RIPA supplemented with PMSF. The cell lysates were collected and centrifuged (10 000–14 000*g*) for 5 minutes to remove the precipitate. The protein concentration was quantified with BCA Protein Assay kit following the manufacturer's protocol. Loaded the same amount of protein in each group and electrophoresed protein on 10% SDS-polyacrylamide gels. The separated proteins were transferred to PVDF membrane of 0.45 μm. The membranes were sealed with skim milk at room temperature for 1 h, then primary antibodies were blotted with proteins at 4 °C over night. After the membranes were washed in TBST for three times, they were incubated with horseradish peroxidase (HRP)-conjugated secondary antibody for 1 h at room temperature, then they were washed thoroughly in TBST. We imaged the membranes with Super Enhancer ECL Kit (Novland, China) on the Chemiluminescence imaging system (Clinx, China) and analyzed them using Image J Software.

2.9 Reverse transcription-PCR (RT-PCR)

ZF4 cells on the NC paper-based chips were cultured for 12 h on the platform of oxygen gradient. The NC paper-based chips were put into EP (Eppendorf) tubes. The cells on the NC paper-based chips were lysed and then total RNA was extracted with Easy Pure RNA Kit. The total RNA was reversely transcribed with TransScript One-Step gDNA Removal and cDNA Synthesis SuperMix Kit. PCR was performed in the PCR Amplifier (Bio-Rad, USA) using Easy Taq PCR Super Mix according to the manufacturer's protocol. The primers used for PCR analysis of $vegf_{165}$ were: sense: 5′-CTCCTCCATCTGTCTGCTGTAAAG-3′ and anti-sense: 5′-CTCTCTGAGCAAGGCTCACAG-3′.[45] The primers of β-actin were: sense: 5′-TTGTAACCAACTGGGACGATATGG-3′, and anti-sense: 5′-GATCTTGATCTTCATGGTGCTAGG-3′.[46] The PCR protocol was executed for 35 cycles and each cycle consisted of denaturation at 95 °C for 30 s, annealing at 55 °C for 30 s, and extension at 72 °C for 30 S. In the initial cycle, samples were incubated at 95 °C for 3 min, in the end of the cycle, samples were incubated at 72 °C for 10 min. The products of PCR were detected by agarose gel electrophoresis and imaged in the Gel Imaging System (JUNYI, China), then the bands were quantified using Image Jo software.

3. Results and discussion

3.1 The characterization of microfluidic chip oxygen gradient platform for cell culture

As shown in Fig. 1 and Fig. S2,† the 3D printed microfluidic chip included a bottom plate and an upper cover plate. A gas-mixing network embedded in the bottom plate, and the gas-mixing networks design rules of 3D printed microfluidic chip were similar to the devices introduced in other studies.[14,35] The gas-mixing networks consisted of two kinds of pipes, serpentine pipes were used to mix the gas by diffusion, and horizontal pipes were used to redistribute gas. The networks were designed to produce a linear gradient of O_2. When one inlet fed N_2, the other fed air, the chip generated air- nitrogen mixtures with $[O_2]$ varying linearly between 0 and 21%.[14,35] Five growth chambers were in the terminal of the gas channel. The gas with different $[O_2]$ flowed over the culture chambers where contain medium, and the cover plate was above the region of cell culture. The two pieces of the chip and soft silicone pad (1.0 mm) were assembled with screws, which formed five separate cell chambers with different oxygen concentrations. Since the gases in the microfluidic network existed as steady states and were continuously renewed, the oxygen concentrations in the cell chamber were stable.[47] The paper-based chips in NC membrane were used as the matrixes for cell culture. NC membrane has small pore size, smooth surface and high hydrophilicity, which makes it an ideal substrate for cell culture and analysis. Unlike PDMS-based microfluidic devices, cells could only rely on fluorescence imaging analysis, the cells on NC paper-based chip in this hybrid platform can be analysed in different ways, for example, flow cytometry assay and western blotting. The NC paper-based chips enabled the 3D-printed microfluidic chip to be reused, each experiment only needs to replace the NC paper-based chips, which reducing the cost of experiments.

3.2 Validation of 3D printed microfluidic chip to generate oxygen gradients

To verify the oxygen gradient profiles within the cell culture chamber of the 3D printed microfluidic chip, we used an oxygen-sensitive fluorescent dye RTDP. RTDP produces strong fluorescence in the absence of oxygen, however, its fluorescence can be quenched by oxygen, so the fluorescent intensity of RTDP decreases as the oxygen content goes up. The oxygen gradient profiles can be described by imaging the fluorescence intensity in the growth chambers while introducing N_2 and air into them. According to eqn (2) and the value of I_0 and I_{air} in Table S1,† K_q was calculated as 58.24. Using the fluorescent intensity of images in Fig. 2A and eqn (1), the $[O_2]$ of each cell culture chamber could be calculated. The results were shown in Table S2.†

According to the calculation formula of $[O_2]$ in the channels: $[O_2] = 5.25\% \times (n\text{-}1)$,[14] the expected $[O_2]$ in channel 1–5 was 0, 5.25%, 10.25%, 15.75% and 21% respectively. The linear relation between $[O_2]$ in each cell culture chamber and the expected $[O_2]$ of respective chamber was good (as shown in Fig. 2B, $R^2 = 0.9825$), which illustrated the 3D printed microfluidic chip we manufactured could generate linear oxygen gradients.

3.3 Culture and identification of fish cells on the platform

To assess the growing situation of cells on the NC paper-based chip, we used live cells fluorescent dye which could make the live cells to generate blue fluorescence. As can be seen from the results in Fig. S6,† a lot of cells on the NC paper-based chips emitted blue fluorescence after 12 h of cultivation, and the cells with blue fluorescence became denser as time extended to 24 h. Cell viability in the 3D printed chip was also tested. As shown in Fig. 3A and C, many cells on the NC paper-based chips cultured in the well-plate and 3D printed chip were stained with live cell dye, and as the culture time increased, the number of live cells increased. The results of cell proliferation assay (Fig. 3B and D) showed that there was no obvious difference in the growth activity between cells cultured in the 3D-printed chip and cells cultured in the well-plate. These results indicated the hybrid platform of NC paper-based chip and 3D-printed chip were suitable for cell culture.

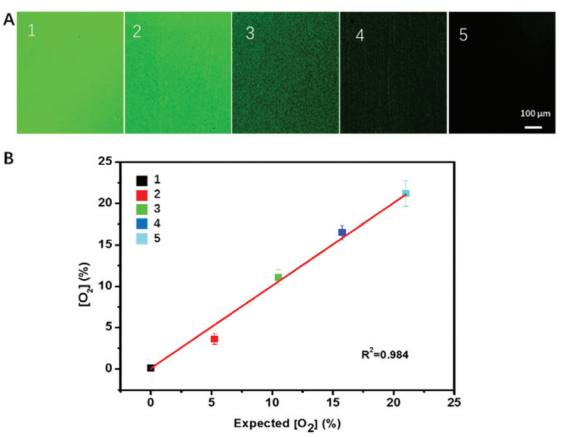

Fig. 2 Concentrations of oxygen generated in 5 channels, as measured by the fluorescence of RTDP in the culture chambers. (A) Fluorescent images of culture chambers 1–5 after RTDP was added to the culture chambers and the system equilibrated for 30 min. (B) Linear relation between the oxygen concentrations measured by RTDP and the expected oxygen concentrations in the channels.

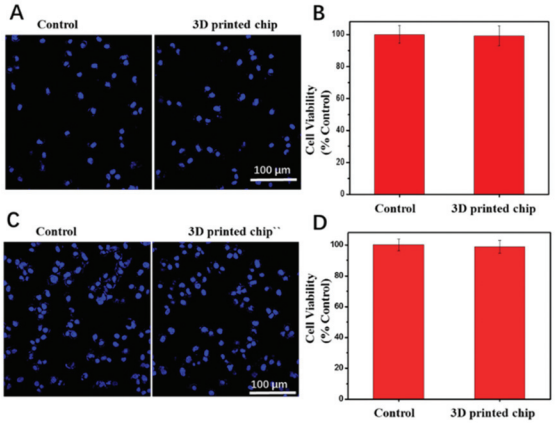

Fig. 3 Cell viability in the 3D printed chip. (A and C) The fluorescent images of ZF4 cells stained with live cell stain reagent after the cells were incubated for 12 h (A) and 24 h (C) in the 3D printed chip. Cells cultured in a well-plate were used as control. (B and D) Cell viability was assessed by the CCK-8 method after ZF4 cells cultured in the 3D printed chip for 12 h (B) and 24 h (D). Cells cultured in a well-plate were used as control.

3.4 Evaluation of intracellular oxygen levels on the oxygen gradient platform

To demonstrate the application of our proposed platform in cell experiments, we cultured zebrafish ZF4 cells in the growth chambers of microfluidic chip, and tested intracellular oxygen levels. Image-iT™ Green Hypoxia Reagent was used to evaluate cellular oxygen level, it is a live-cell permeable compound, and its fluorescence increases in environments with low oxygen concentrations.[43] As shown in Fig. 4A and B, the cells almost had no fluorescence when the $[O_2]$ was 21% and 15.75%, and the intracellular fluorescence was very weak in the environment of 10.5% $[O_2]$. However, the cellular fluorescence began to increase in 5.25% $[O_2]$, and strong cellular fluorescence was observed when the $[O_2]$ was 0%. Quantification of the fluorescence intensity demonstrated that the cellular fluorescence increased gradually along with the decrease of $[O_2]$. Considering that a relatively small number of cells could be analysed in the fluorescence imaging, we further detect the density of the cellular fluorescence in each channel with flow cytometry. The flow cytometry can analyse millions of cells in a short time and produce statistical results, so it has stronger analytical reliability. In Fig. 4C and D, the *Y*-axis of the histogram was the cell counts and the *X*-axis was the fluorescence intensity of hypoxia reagent in logarithmic form. The peak of histogram moved more and more to the right with the

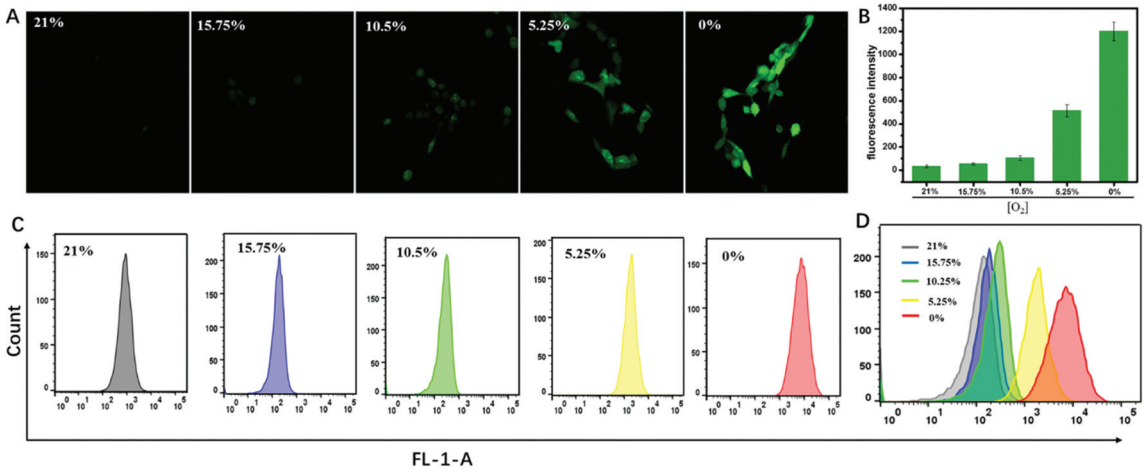

Fig. 4 Fluorescence images and flow cytometry detection of cellular oxygen levels on the oxygen gradient platform. (A) Fluorescent images of cellular oxygen levels after ZF4 cells were cultured in different channels on the platform for 4 h, fluorescence signal resulting from Image-iT™ Green Hypoxia Reagent, the excitation wavelength was 488 nm and collection wavelength was 500–600 nm. (B) Quantitative results of fluorescence intensity for each group in (A). (C) Flow cytometry results of cellular oxygen levels after ZF4 cells were cultured in different channels on the platform for 4 h. (D) Overlays of histograms in (C).

decrease of $[O_2]$ in the growth chambers. As shown in Fig. 4D, the overlays of histogram in five channels showed great differences from each other. The results obtained by flow cytometry were in good consistency with those obtained by fluorescence imaging, which indicated the cellular oxygen level in the channels of the hybrid microfluidic platform presented a gradient.

3.5 Hypoxia caused cellular stress response

Reactive oxygen species (ROS) are cellular signal molecules synthesized in cells in response to metabolic processes. Hypoxia stress induces the production of reactive oxygen species (ROS) in cells,[44] which is a main cause of cell damage or apoptosis. We used fluorescent probe (DCFH-DA) of ROS to investigate the change of cellular ROS under different hypoxia stress. As illustrated in Fig. 5A and B, the position of the histogram moved to the right along with the decrease of oxygen content, which indicated intercellular ROS increased with the increasing degree of hypoxia in the channel. Hypoxia-inducible factor 1 (HIF1) is a heterodimeric transcription factor that plays an important role in the cellular response to hypoxia stress. It consists of HIF-1α and HIF-1β subunits.[48] HIF1 regulates the transcription of many genes including genes regulating angiogenesis, erythropoiesis, cell cycle, metabolism and apoptosis,[49] which could accelerate responses to the hypoxic environment. HIF-1α is degraded rapidly in normoxic cells, however, hypoxia retards HIF-1α degradation and lead to its accumulation in cells,[50] and HIF-1α is therefore only found in hypoxic cells. We examined cellular HIF-1α by western blot after ZF4 cells cultured under different hypoxic conditions for 4 h. As shown in Fig. 5C and D, the content of intracellular

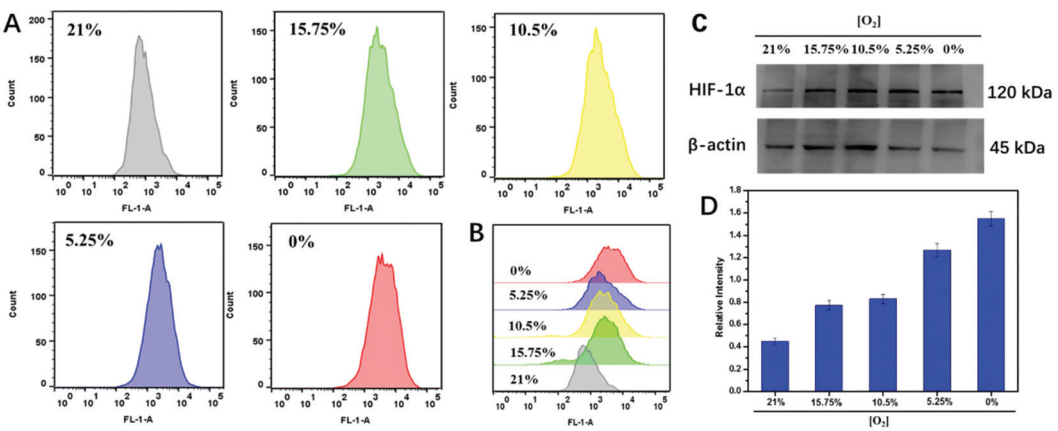

Fig. 5 The change of intracellular ROS and HIF-1α under different O_2 levels. (A) Histograms of flow cytometry for detecting cellular ROS after ZF4 cells were cultured for 4 h under different concentrations of O_2. (B) The overlays of histograms in (A). (C) Western blot analysis of intracellular HIF-1α after ZF4 cells were cultured for 4 h under different concentrations of O2. β-Actin was taken as the loading reference. (D) The quantitative analysis of HIF-1α and β-actin stripes.

HIF-1α in channel gradually increased along with the oxygen concentration decreasing. The above results indicate that both ROS and HIF-1α were upregulated under hypoxic stress during 4 h. This phenomenon can be attributed to the intracellular stress response caused by hypoxia.[44,49]

3.6 Hypoxia activated the transcription of vascular endothelial growth factor (VEGF) in zebrafish cells

Vascular endothelial growth factor (VEGF) is an effective factor that promotes angiogenesis. VEGF and its tyrosine kinase receptor have been confirmed to play important roles in embryonic and tumor angiogenesis.[51] It has been reported that $Vegf_{165}$ and $Vegf_{121}$ are the main expression forms in zebrafish embryos.[51] To study the impact of hypoxia on cellular VEGF of zebrafish, the mRNA expression level of $vegf_{165}$ was quantitatively analysed using RT-PCR method after ZF4 cells were exposed to different oxygen tensions on the platform of oxygen gradient for 12 hours. As a control, a housekeeping gene, β-actin was also analysed by RT-PCR using a pair of β-actin specific primers. As shown in Fig. 6, VEGF mRNA expression levels increased as the oxygen level in the channel decreased, which indicated hypoxia activated the transcription of vascular endothelial growth factor. *In vitro* studies of mammalian systems revealed that many inducible genes are regulated by a ubiquitous DNA-binding protein hypoxia inducible factor 1 (HIF-1). In mammal and fish, HIF-1 receives signals from the molecular oxygen sensor through redox reactions and/or phosphorylation. HIF-1α then activates the transcription of a number of hypoxia-inducible genes, including: vascular endothelial growth factor (VEGF),[4] which to enhance proliferation of blood vessels for increasing oxygen supply.[52] Our results revealed that hypoxia induced hypoxia-inducible factor 1α (HIF-1α) accumulate, and HIF-1α in turn stimulates the transcription of hypoxia-responsive genes VEGF in the ZF4 cells of zebrafish.

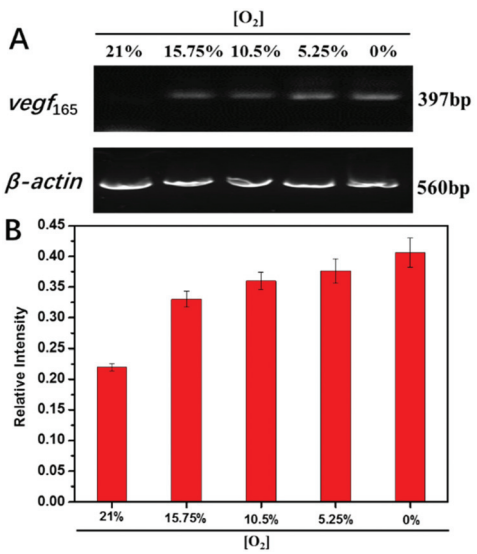

Fig. 6 RT-PCR analysis of zebrafish cellular *vegf* expression. (A) RT-PCR analysis of zebrafish cellular $vegf_{165}$ expression under different O_2 levels. Standard loading was indicated by β-actin expression. (B) The relative intensity analysis of $vegf_{165}$ and β-actin expressions shown in (A).

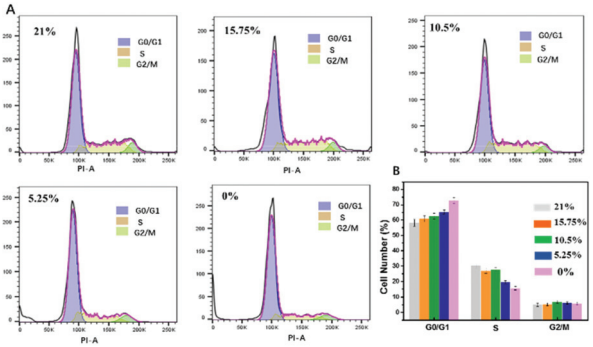

Fig. 7 Hypoxia induce cell cycle arrest to zebrafish cells. (A) Cell cycle histogram of ZF4 cells under different O_2 levels. The cell cycle phase analysis was performed by flow cytometry after cells cultured on the of the oxygen gradient platform for 12 h. (B)The statistics of ZF4 cells in channels 1–5 in G0/G1, S and G2/M phase.

3.7 Hypoxia caused cell cycle arrest in zebrafish cells

In mammalian cells, hypoxia can change the course of the cell cycle by HIFs (hypoxia-inducible factors) whose transcriptional targets are present in cell cycle regulation.[53] In order to determine the effect of hypoxia on cycle progression of fish cells, ZF4 cells were exposed to different oxygen tensions on the platform of oxygen gradient for 12 hours, and intracellular DNA content was analysed by PI staining. As shown in Fig. 7A, the results of flow cytometric analysis, the *Y*-axis of the histogram was the cell counts and *X*-axis was the DNA content of different cell phase. DNA histograms revealed that there was a change in the cell cycle distribution of ZF4 cells. The statistical results indicated that the proportion of G0/G1 phase increased as the decreasing oxygen levels in the channels (Fig. 7B), which indicated hypoxia induced cell cycle arrest at G0/G1 phase. The results of Fig. 5C and D showed that hypoxia also caused intracellular HIF-1α increasing. These results indicated that HIF-1α accumulation under hypoxic conditions would be responsible for the hypoxia-induced cell cycle arrest, which was reported in other research.[49] The cell proliferation could be repressed through blocking cell cycle progression, this stress response is essential for maintenance of cell viability under hypoxia.

4. Conclusion

This work developed a platform integrating 3D printing and nitrocellulose -based microfluidic chip to investigate the effect of oxygen gradient on cells. This platform could generate steady oxygen gradient for cells in short time (30 min). Compared with conventional PDMS chips of oxygen gradient for cell cultures that can only rely on fluorescence microscope analysis, this hybrid nitrocellulose-based microfluidic platform

can provide a variety of analysis methods for cells, including flow cytometry, western blot and RT-PCR, which greatly expands the application potential of microfluidic chips. To better illustrate the performance and application of this platform, it was applied in studying the effect of oxygen gradient on fish cells. Hypoxia caused the increase of intercellular ROS and HIF-1α accumulation, HIF-1α in turn stimulates the transcription of hypoxia-responsive genes VEGF in the ZF4 cells of zebrafish. Hypoxia also caused cell cycle arrest in zebrafish cells, which could lead to cell growth repression. This 3D-printed nitrocellulose microfluidic device could provide a low-cost and user-friendly route for cell research under different oxygen environments. It is expected that this hybrid platform has good potential for detecting the responses of cells to oxygen gradient in many fields.

Author contributions

Ping Liu: investigation, methodology, writing original draft. Longwen Fu: investigation, data curation. Zhihua Song: investigation, methodology. Mingsan Man: methodology. Huamao Yuan: data curation, investigation. Xiaoli Zheng: methodology. Qi Kang: investigation, formal analysis. Jinming Song: investigation, funding acquisition. Dazhong Shen: investigation, supervision, writing–review& editing. Bowei Li: conceptualization, project administration, writing–review & editing. Lingxin Chen: supervision, resources, funding acquisition, writing–review & editing.

Conflicts of interest

The authors declare that they have no conflict of interest.

Acknowledgements

This work was financially supported by the National Natural Science Foundation of China (Grant No. 41776110; 21976209; 21874083), the National Key Research and Development Program of China (Grant No. 2016YFC1400702), Key Deployment Project of Centre for Ocean Mega-Research of Science, Chinese Academy of Sciences (COMS2019J01), and Open Fund of CAS Key Laboratory of Marine Ecology and Environmental Sciences, Institute of Oceanology, Chinese Academy of Sciences (KLMEES202002).

References

1 D. Breitburg, L. A. Levin, A. Oschlies, M. Gregoire, F. P. Chavez, D. J. Conley, V. Garcon, D. Gilbert, D. Gutierrez, K. Isensee, G. S. Jacinto, K. E. Limburg, I. Montes, S. W. A. Naqvi, G. C. Pitcher, N. N. Rabalais, M. R. Roman, K. A. Rose, B. A. Seibel, M. Telszewski, M. Yasuhara and J. Zhang, *Science*, 2018, **359**, 46–56.
2 A. G. Keppel, D. L. Breitburg, G. H. Wikfors, R. B. Burrell and V. M. Clark, *Mar. Ecol.: Prog. Ser.*, 2015, **538**, 169–183.
3 K. L. Stierhoff, T. E. Targett and J. H. Power, *Can. J. Fish. Aquat. Sci.*, 2009, **66**, 1033–1047.
4 R. S. S. Wu, *Mar. Pollut. Bull.*, 2002, **45**, 35–45.
5 M. D. Brennan, M. L. Rexius-Hall, L. J. Elgass and D. T. Eddington, *Lab Chip*, 2014, **14**, 4305–4318.
6 H. J. Chiang, S. L. Yeh, C. C. Peng, W. H. Liao and Y. C. Tung, *J. Visualized Exp.*, 2017, **120**, e55292.
7 Y. A. Chen, A. D. King, H. C. Shih, C. C. Peng, C. Y. Wu, W. H. Liao and Y. C. Tung, *Lab Chip*, 2011, **11**, 3626–3633.
8 C. W. Chang, Y. J. Cheng, M. Tu, Y. H. Chen, C. C. Peng, W. H. Liao and Y. C. Tung, *Lab Chip*, 2014, **14**, 3762–3772.
9 Y. Li, L. Li, Z. Liu, M. Ding, G. Luo and Q. Liang, *Microfluid. Nanofluid.*, 2016, **20**, 971–979.
10 K. Yang, S. Han, Y. Shin, E. Ko, J. Kim, K. I. Park, S. Chung and S. W. Cho, *Biomaterials*, 2013, **34**, 6607–6614.
11 J. F. Lo, E. Sinkala and D. T. Eddington, *Lab Chip*, 2010, **10**, 2394–2401.
12 S. C. Oppegard, A. J. Blake, J. C. Williams and D. T. Eddington, *Lab Chip*, 2010, **10**, 2366–2373.
13 K. Funamoto, I. K. Zervantonakis, Y. Liu, C. J. Ochs, C. Kim and R. D. Kamm, *Lab Chip*, 2012, **12**, 4855–4863.
14 M. Polinkovsky, E. Gutierrez, A. Levchenko and A. Groisman, *Lab Chip*, 2009, **9**, 1073–1084.
15 P. Liu, B. W. Li, L. W. Fu, Y. Huang, M. S. Man, J. Qi, X. Y. Sun, Q. Kang, D. Z. Shen and L. X. Chen, *ACS Sens.*, 2020, **5**, 464–473.
16 C. M. Ho, S. H. Ng, K. H. Li and Y. J. Yoon, *Lab Chip*, 2015, **15**, 3627–3637.
17 A. I. Shallan, P. Smejkal, M. Corban, R. M. Guijt and M. C. Breadmore, *Anal. Chem.*, 2014, **86**, 3124–3130.
18 A. K. Au, W. Huynh, L. F. Horowitz and A. Folch, *Angew. Chem., Int. Ed.*, 2016, **55**, 3862–3881.
19 N. Bhattacharjee, A. Urrios, S. Kanga and A. Folch, *Lab Chip*, 2016, **16**, 1720–1742.
20 K. Tenda, B. van Gerven, R. Arts, Y. Hiruta, M. Merkx and D. Citterio, *Angew. Chem., Int. Ed.*, 2018, **57**, 15369–15373.
21 J. Qi, B. Li, N. Zhou, X. Wang, D. Deng, L. Luo and L. Chen, *Biosens. Bioelectron.*, 2019, **142**, 111533–111533.
22 K. Maejima, Y. Hiruta and D. Citterio, *Anal. Chem.*, 2020, **92**, 4749–4754.
23 C. C. Liu, Y. N. Wang, L. M. Fu and Y. H. Huang, *Chem. Eng. J.*, 2018, **332**, 695–701.
24 D. Lin, B. W. Li, J. Qi, X. F. Ji, S. X. Yang, W. H. Wang and L. X. Chen, *Sens. Actuators, B*, 2020, **303**, 127213–127220.
25 K. Yamada, T. G. Henares, K. Suzuki and D. Citterio, *Angew. Chem., Int. Ed.*, 2015, **54**, 5294–5310.
26 J. Qi, B. W. Li, X. R. Wang, Z. Zhang, Z. Wang, J. L. Han and L. X. Chen, *Sens. Actuators, B*, 2017, **251**, 224–233.
27 R. D. Liu, E. M. McConnell, J. X. Li and Y. F. Li, *J. Mater. Chem. B*, 2020, **8**, 3213–3230.
28 B. Mosadegh, M. R. Lockett, K. T. Minn, K. A. Simon, K. Gilbert, S. Hillier, D. Newsome, H. Li, A. B. Hall, D. M. Boucher, B. K. Eustace and G. M. Whitesides, *Biomaterials*, 2015, **52**, 262–271.

29 H. J. Park, S. J. Yu, K. Yang, Y. Jin, A. N. Cho, J. Kim, B. Lee, H. S. Yang, S. G. Im and S. W. Cho, *Biomaterials*, 2014, **35**, 9811–9823.
30 K. A. Simon, B. Mosadegh, K. T. Minn, M. R. Lockett, M. R. Mohammady, D. M. Boucher, A. B. Hall, S. M. Hillier, T. Udagawa, B. K. Eustace and G. M. Whitesides, *Biomaterials*, 2016, **95**, 47–59.
31 B. Mosadegh, B. E. Dabiri, M. R. Lockett, R. Derda, P. Campbell, K. K. Parker and G. M. Whitesides, *Adv. Healthcare Mater.*, 2014, **3**, 1036–1043.
32 R. Bai, L. Li, M. Liu, S. Yan, C. Miao, R. Li, Y. Luo, T. Liu, B. Lin, Y. Ji and Y. Lu, *Anal. Chem.*, 2018, **90**, 5825–5832.
33 Y. Lu, W. W. Shi, J. H. Qin and B. C. Lin, *Anal. Chem.*, 2010, **82**, 329–335.
34 L. Wang, C. Xu, Y. J. Zhu, Y. Yu, N. Sun, X. Q. Zhang, K. Feng and J. H. Qin, *Lab Chip*, 2015, **15**, 4283–4290.
35 K. Campbell and A. Groisman, *Lab Chip*, 2007, **7**, 264–272.
36 D. Gao, H. F. Li, N. J. Wang and J. M. Lin, *Anal. Chem.*, 2012, **84**, 9230–9237.
37 M. S. Jie, S. F. Mao, H. F. Li and J. M. Lin, *Chin. Chem. Lett.*, 2017, **28**, 1625–1630.
38 M. Adler, M. Polinkovsky, E. Gutierrez and A. Groisman, *Lab Chip*, 2010, **10**, 388–391.
39 Y. A. Chen, A. D. King, H. C. Shih, C. C. Peng, C. Y. Wu, W. H. Liao and Y. C. Tung, *Lab Chip*, 2011, **11**, 3626–3633.
40 G. Mehta, K. Mehta, D. Sud, J. W. Song, T. Bersano-Begey, N. Futai, Y. S. Heo, M. A. Mycek, J. J. Linderman and S. Takayama, *Biomed. Microdevices*, 2007, **9**, 123–134.
41 B. W. Li, Z. Zhang, J. Qi, N. Zhou, S. Qin, J. Choo and L. X. Chen, *ACS Sens.*, 2017, **2**, 243–250.
42 B. Li, J. Qi, L. Fu, J. Han, J. Choo, A. J. deMello, B. Lin and L. Chen, *Biosens. Bioelectron.*, 2020, **165**, 112282.
43 S. Barmaki, V. Jokinen, D. Obermaier, D. Blokhina, M. Korhonen, R. H. A. Ras, J. Vuola, S. Franssila and E. Kankuri, *Acta Biomater.*, 2018, **73**, 167–179.
44 M. Gao, R. Wang, F. B. Yu and L. X. Chen, *Biomaterials*, 2018, **160**, 1–14.
45 D. Liang, X. Z. Xu, A. J. Chin, N. V. Balasubramaniyan, M. A. L. Teo, T. J. Lam, E. S. Weinberg and R. W. Ge, *Biochim. Biophys. Acta, Gene Struct. Expression*, 1998, **1397**, 14–20.
46 L. D. Jensen, Z. Q. Cao, M. Nakamura, Y. L. Yang, L. Brautigam, P. Andersson, Y. Zhang, E. Wahlberg, T. Lanne, K. Hosaka and Y. H. Cao, *Cell Rep.*, 2012, **2**, 231–241.
47 S. K. W. Dertinger, D. T. Chiu, N. L. Jeon and G. M. Whitesides, *Anal. Chem.*, 2001, **73**, 1240–1246.
48 F. R. Sharp and M. Bernaudin, *Nat. Rev. Neurosci.*, 2004, **5**, 437–448.
49 C. X. Huang, N. Chen, X. J. Wu, Y. He, C. H. Huang, H. Liu, W. M. Wang and H. L. Wang, *Life Sci.*, 2017, **171**, 21–29.
50 M. Ohh, C. W. Park, N. Ivan, M. A. Hoffman, T. Y. Kim, L. E. Huang, N. Pavletich, V. Chau and W. G. Kaelin, *Nat. Cell Biol.*, 2000, **2**, 423–427.
51 D. Liang, J. R. Chang, A. J. Chin, A. Smith, C. Kelly, E. S. Weinberg and R. W. Ge, *Mech. Dev.*, 2001, **108**, 29–43.
52 Z. Arany, L. E. Huang, R. Eckner, S. Bhattacharya, C. Jiang, M. A. Goldberg, H. F. Bunn and D. M. Livingston, *Proc. Natl. Acad. Sci. U. S. A.*, 1996, **93**, 12969–12973.
53 W. Jeong, S. Jung, F. W. Bazer and J. Kim, *Theriogenology*, 2018, **115**, 9–15.